Motion of interacting defects in the Ginzburg-Landau model

J. D. Rodriguez and L. M. Pismen
Department of Chemical Engineering, Technion, Haifa 32000, Israel

L. Sirovich
Division of Applied Mathematics, Brown University, Providence, Rhode Island 02912
(Received 18 March 1991; revised manuscript received 1 July 1991)

Velocities and trajectories of interacting defects in the real Ginzburg-Landau equation are obtained by applying equations of motion of defects under the influence of the local phase field in conjunction with the Green's-function solution of the heat equation governing the phase field generated by moving defects.

PACS number(s): 05.70.Ln, 47.20.Ky, 03.40.Kf

The rational approach to the description of realistic nonequilibrium patterns in extended systems, which allows one to avoid short-scale computations using fine grids, is based on the "particle-field" approximation. The role of particles is played by topological defects whose interaction is mediated by gauge fields corresponding to the symmetry group of the order-parameter space. In order to realize this approach, one needs to first obtain equations of motion of defects under the influence of the local field. Then the field equations have to be solved simultaneously with these equations of motion to obtain the evolution of both the field and the positions of defects.

The first task has been completed in the simplest case of the dissipative Ginzburg-Landau (GL) equation:

$$u_t = \nabla^2 u + (1 - |u|^2)u. \tag{1}$$

This equation provides an adequate model for convective patterns when a definite orientation of convection rolls is induced by the boundary conditions, as occurs, for example, in the case of electroconvection in liquid crystals [1, 2]. The lowest energy state is achieved when the real amplitude $\rho = |u|$ equals unity. The system is symmetric with respect to the translations of the phase $\theta = \arg u$. When the phase varies on an extended spatial and temporal scale, the amplitude follows the phase adiabatically. As a consequence, the nonlinear GL equation can be replaced, in the long-scale approximation, by the heat equation describing the slow phase evolution:

$$\theta_t = \nabla^2 \theta. \tag{2}$$

The phase description breaks down in the vicinity of defects that are characterized by the circulation condition

$$\oint_\gamma \nabla\theta = 2\pi n, \tag{3}$$

where the integration is carried out over an arbitrary contour γ enclosing the defect. Stable defects carry the topological charge $n = \pm 1$.

The mobility of point defects in the plane under the action of a small phase gradient was computed by Bodenschatz, Pesch, and Kramer [1]. Their approach uses a representation of the defect velocity as the ratio of the Peach-Köhler force to the dissipation integral. The integral is then evaluated by using asymptotic forms of the defect solution in the near- and far-field limits. In the immediate vicinity of the defect, the authors use the stationary symmetric solution of the full GL equation; and in the far field, a stationary solution of the phase equation in the coordinate frame comoving with the defect. This result was confirmed by Pismen and Rodriguez [3] using the method of matched asymptotic expansions. The relation between the defect velocity v, directed normally to the acting phase gradient, and the latter's magnitude $A = |\nabla\theta|$ reads

$$A = \frac{v}{2} \ln \frac{v_0}{v}, \quad v_0 = 3.29. \tag{4}$$

Equation (4) can be seen as the first ingredient of the "particle-field" description. Being local, i.e., dependent on the value of the external gradient at the core of the defect, it should remain valid also when the gradient is slowly changing in time and space. It is not, however, sufficient by itself to solve the problem of defect interaction. We recall that the phase field of a moving defect is velocity dependent [1, 3]:

$$\theta_x = A + \frac{v}{2} \exp\left(-\frac{vr}{2}\sin\phi\right)\left[K_0\left(\frac{vr}{2}\right) - \sin\phi\, K_1\left(\frac{vr}{2}\right)\right],$$
$$\theta_y = \frac{v}{2} \exp\left(-\frac{vr}{2}\sin\phi\right)\cos\phi\, K_1\left(\frac{vr}{2}\right), \tag{5}$$

where r, ϕ are polar coordinates centered on the moving defect and K_n are modified Bessel functions. When defects are in motion, the phase field induced by each defect at the core of another depends, strictly speaking, on its entire past history of accelerations. Thus, solving the *nonstationary* phase equation is necessary.

In Ref. [3], the "self-consistent" approximation was used instead, and the velocity was found by assuming that the quasistationary phase field corresponding to the instantaneous velocity is observed at each location. Un-

der this assumption, the migration velocity (as a function of the instantaneous separation between the vortex cores) is obtained by first computing the value of the phase gradient due to one of the vortices at the core of another, using Eqs. (5). The velocity is then given by the mobility relationship (4). For oppositely charged defects moving towards each other, the phase gradient generated by one of the defects at the core of the other is $\theta_x(r, \frac{1}{2}\pi)$, while for like-charged defects, moving apart, it is $\theta_x(r, -\frac{1}{2}\pi)$. Quasistationary velocities are computed then as solutions of the equation

$$\ln \frac{v_0}{v} = e^{\pm vr/2} \left[K_0 \left(\frac{vr}{2} \right) \pm K_1 \left(\frac{vr}{2} \right) \right], \tag{6}$$

where the positive sign should be taken for the repelling and the negative sign for the attracting pair of vortices. At separations larger than a certain minimum $r_c = O(1)$, two branches of solutions exist, of which the lower one, corresponding to velocities decreasing with separation, is physical.

The self-consistent solution was introduced as an estimate rather than as a rational approximation, though it was expected to work well when the separation is very large even on the extended scale. The correct way to determine the evolution of the system is to integrate the phase equation (2) subject to the circulation condition (3) on the defects moving under the influence of the local phase gradient according to Eq. (4).

Since the phase equation is linear, its solution can be presented as a superposition $\theta = \sum_i \theta_i$ of phase fields θ_i generated by different defects and subject to the respective circulation conditions. For the latter fields, it appears to be possible to write down solutions corresponding to arbitrary defect trajectories with the help of an appropriate Green's function. A difficulty arises, however, due to the multivalued nature of θ_i. It is convenient therefore to introduce univalued functions dual to θ_i that would obey a usual heat equation with a point source located at the defect.

We shall restrict our study to the motion of a pair of defects. In this case, the motion is rectilinear, and may be assumed without loss of generality to be along the y axis. Then the dual function $\Phi(x, y, t)$ is defined by

$$\theta_x = \Phi_y + v\Phi - \int^y \Phi_t dy, \quad -\theta_y = \Phi_x. \tag{7}$$

One can see that the equation

$$\Phi_{xx} + \Phi_{yy} + v\Phi_y - \Phi_t = 2\pi\delta(x)\delta(y) \tag{8}$$

both serves as the integrability condition for θ in (7) and ensures that the circulation condition (3) be satisfied. The dual function can be expressed using the Green's function of Eq. (8) as

$$\Phi = \frac{1}{2} \int_0^t (t-s)^{-1} \exp \left(-\frac{[y + q(t) - q(s)]^2}{4(t-s)} \right) ds. \tag{9}$$

Here $q(t)$ is the instantaneous position of the defect moving along the axis $x = 0$. The phase gradient computed from (9) and (7) is further used in the mobility relationship (4) to obtain the velocities and subsequent positions of the defects.

The illustrations show numerical results of computations utilizing the above procedure. We start with the case of a pair of defects of the opposite sign moving towards one another in an unbounded domain from some initial distance to annihilate at the point $y = 0$. Due to the symmetry, it is sufficient to consider a single defect together with its image in a reflecting wall placed at $y = 0$. Ideally, the interacting defects should be nucleated at an infinite separation distance. For a practical numerical calculation the integration must start from a finite separation, and hence there is some uncertainty in the choice of initial conditions. We take as the initial phase distribution that corresponding to the self-consistent solution. The dependence $v(r)$ of the velocity on instantaneous separation is shown by the solid line in Fig. 1. For comparison, the dashed line in the same figure shows the quasistationary self-consistent dependence (6) and the dotted line, a "solid-body" solution computed under the assumption that one of the defects moves in the unchanging phase field of the other. The "solid-body" and self-consistent velocities correspond to the defect motion in the respective limits of infinite and zero acceleration. These two limits thus define the bounds of the numerically computed velocity. The $v(r)$ dependence in Fig. 2 was computed using the initial conditions of a phase field rapidly decaying outside the defects. As we see in this case also, velocities of defects starting from different separations closely approach the self-consistent values. In all cases, the defects accelerate steeply at close approach, and computations have to stop shortly before the moment of annihilation when the basic assumptions of slow motion and weak phase gradients are no longer valid.

In computations of the $v(r)$ curves shown Fig. 3, we imposed, in addition to the defect interaction, an external phase gradient driving the vortices towards annihilation. The motion starts with the stationary velocity corresponding to the driving gradient, and gradually accelerates as the vortices draw closer to each other. Figure

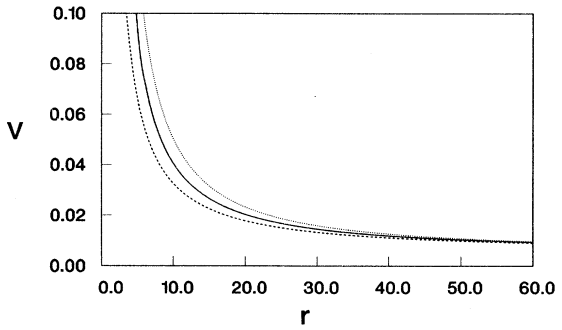

FIG. 1. The dependence of the velocity on distance for a pair of interacting defects of the opposite sign, starting, at a certain distance, from a self-consistent phase field, and eventually annihilating. The solid line shows the computed $v(r)$ curve. The dashed line shows the self-consistent approximation, and the dotted line the "solid-body" approximation (with the initial phase unchanged).

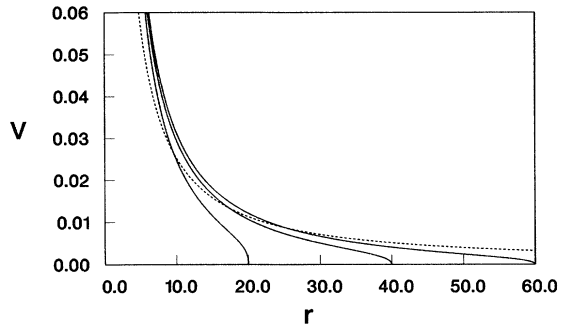

FIG. 2. Annihilating defects, starting from zero phase at different distances. The dashed line shows the self-consistent $v(r)$ curve.

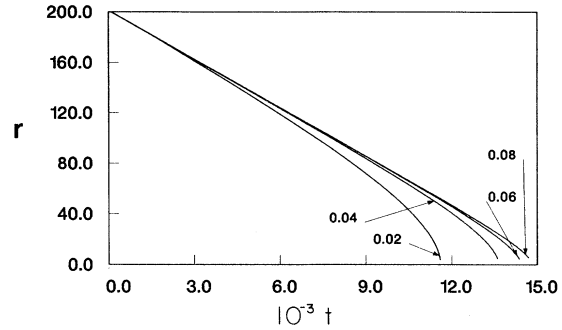

FIG. 4. The defects separation vs time for annihilating defects accelerated by an external phase gradient. All curves, labeled by the value of the external gradient, are brought together by rescaling the data in such a way that initial velocities coincide.

4, based on the same computations, shows the change in time of the positions of one of the defects relative to their common center of gravity. All curves have been brought together by rescaling the data in such a way that initial velocities coincide.

In order to compare with experimental results, suitable rescalings must first be introduced. The spatial variables are rescaled by the coherence lengths ξ_1 and ξ_2, for the directions perpendicular and parallel to the roll axis, respectively. Similarly, time is rescaled by the relaxation time T_0. The phase gradient A corresponds to the wave-number mismatch $q - q_c$ which represents the deviation from the threshold wave vector q_c, and gives rise to the Peach-Köhler force.

Given an experimentally determined velocity V, with components V_x and V_y, the dimensionless velocity is determined as [1]

$$v = T_0(V_x^2\xi_2^2 + V_y^2\xi_1^2 - 2a\xi_1\xi_2V_xV_y)^{1/2} \times(\xi_1\xi_2\sqrt{1-a^2}\epsilon^{1/2})^{-1},$$

where ϵ represents the perturbation of the system above the threshold and a is a global rotation parameter, such that $a = 0$ for normal roll patterns and $0 \leq a < 1$ for oblique rolls.

A comparison with the experimental results of Braun and Steinberg [4] is shown in Fig. 5. The experimental data represent climbing motion of a pair of defects. Since the wave-number mismatch has been not measured in the experiment, we recovered this value by extrapolating the data to the asymptotic velocity and computing the corresponding value of A using Eq. (4). The lower curve corresponds to a value of $\epsilon = 0.05$; a fit of this data indicates an asymptotic velocity of 0.019 and a wave-number mismatch $A = 0.05$. The upper curve represents data for $\epsilon = 0.04$ with an asymptotic velocity of 0.060 and $A = 0.12$. The numerical solution was then generated by nucleating a pair of defects at a large initial separation, to allow a suitable time interval for the phase field to evolve into a close approximation of the quasisteady field while mutual interaction was still negligible. The computed acceleration close to the annihilation point is somewhat more gradual than in the experiment, but the quantitative comparison is difficult due to both uncertainty of experimental data and possible deviations of the experimental system from the idealized Ginzburg-Landau model.

Figure 6 shows the $v(r)$ curves for the case when a pair of defects of the opposite sign nucleate and move apart under the action of an external phase gradient. Computations start at a separation in the immediate vicinity of an unstable bound state where the driving gradient

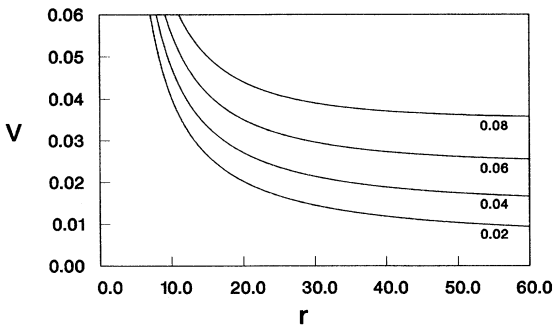

FIG. 3. Annihilating defects accelerated by an external phase gradient. The curves are labeled by the values of the gradient A.

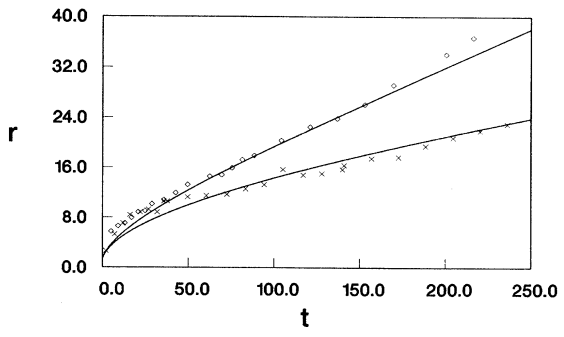

FIG. 5. The defects separation vs time for annihilating defects accelerated by an external phase gradient. The experimental points shows the rescaled data defects from Ref. [4].

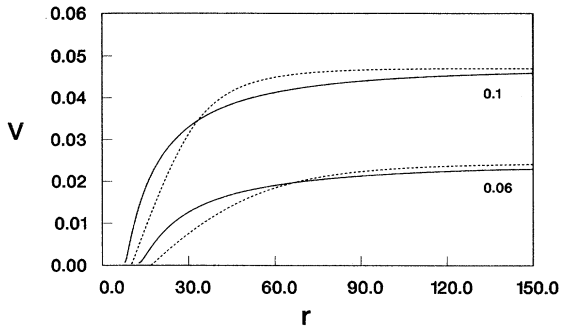

FIG. 6. Nucleation of a pair of defects under external phase gradient. The computed curves (solid) are labeled by the values of the gradient A. The dashed lines show self-consistent velocities.

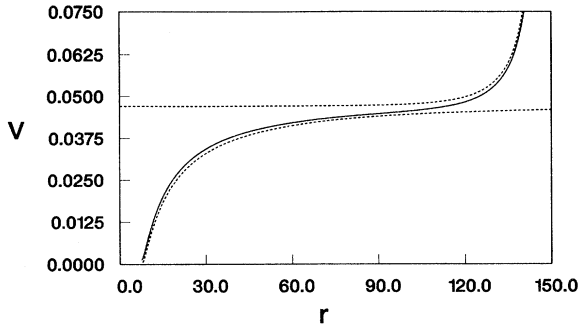

FIG. 8. Nucleation of a pair of defects under external phase gradient ($A = 0.1$) and annihilation at the wall (solid line), compared with the nucleation (in the left) and the annihilation (in the right) in the infinite domain (dashed lines).

is nearly compensated by the attraction, and velocities are very small. Consequently, the diverging defects accelerate, approaching stationary velocities corresponding to the given gradients when separations are large. Self-consistent velocities, shown by dashed lines in the same figure, are reasonably close to computational results.

Since the far-field phase equation is a linear heat equation, the presence of sidewall boundaries may be dealt with by the use of image defects. The simplest cases that can be considered each involve two sidewalls. The location of sidewalls and images for domains bounded in the x and y directions, respectively, are shown in Fig. 7, indicating also signs of the image charges.

Figure 8 shows the effect of sidewalls in the x direction (perpendicular to the direction of propagation). Also shown in this figure are the corresponding $v(r)$ curves for the infinite domain case. The solid finite domain curve is quite close to a combination of the broken curves corresponding to the nucleation (in the left) and to the annihilation with the image (in the right) in the infinite domain.

The influence of lateral walls (parallel to the y axis) is more substantial. We shall consider the case when defects of the opposite sign nucleate and move apart under the action of an external phase gradient. The total phase gradient at a point $(0, \frac{r}{2})$ is given by the sum over the

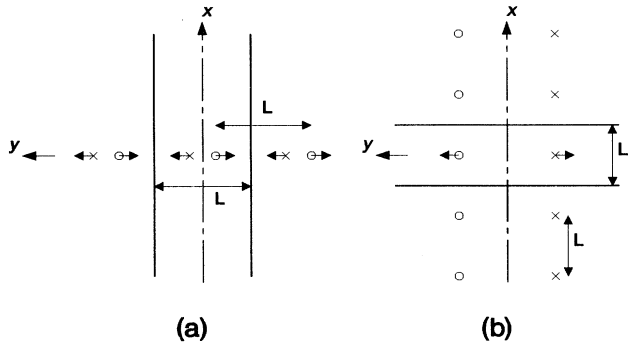

FIG. 7. Configuration of sidewalls normal (a) and parallel (b) to the direction of motion. Markers × and ○ indicate the polarity of defects and images.

image defects. These consists of two rows, one each at $y = \pm\frac{r}{2}$. The defects at $(\pm nL, \frac{r}{2})$ and $(\pm nL, -\frac{r}{2})$ act to accelerate and decelerate the defect, respectively.

If the motion is stationary, the driving phase field created at the core of the defect at $(0, \frac{r}{2})$ by the image at $(nL, \frac{r}{2})$ can be written using the function $\theta_x(r, \phi)$ in Eq. (5) as $\theta_x(nL, 0) = \theta_x(nL, \pi) = \frac{v}{2} K_0\left(\frac{nvL}{2}\right)$. Summing over all images, we deduce that the phase gradient due to the row of images at $y = \frac{r}{2}$ is given by $A_+ = v\sum_{n=1}^{\infty} K_0\left(\frac{vnL}{2}\right)$. As the defect separation becomes large, one might be tempted to neglect the contribution of the images at $(\pm nL, -\frac{r}{2})$ since the phase gradient contribution of each image approaches zero as $r \to \infty$. Interestingly enough, however, the contribution of this row of images does not vanish for large defect separations. Furthermore, we shall see that this contribution to the effective phase-gradient dominates the contribution of the defects at $(\pm nL, \frac{r}{2})$.

Using the asymptotics of the Bessel functions for large argument, we may write the phase-gradient contribution from the images at $(\pm nL, -\frac{r}{2})$ as

$$A_- = \sqrt{\pi v}\sum_{n=1}^{N(r)} \frac{1}{(r^2 + n^2L^2)^{1/4}}\left(1 + \frac{r}{\sqrt{r^2 + n^2L^2}}\right) \times \exp\left(-\frac{v}{2}(\sqrt{r^2 + n^2L^2} + r)\right).$$

To proceed, we truncate the above sum at some suitably large $n = N$. In general, this value will be a function of r. For the defect at $(NL, -\frac{r}{2})$ to have a nonvanishing contribution to the total gradient at $(0, \frac{r}{2})$, the angle given by $\tan^{-1}(\frac{y}{2NL})$ must be small, since the phase gradient decays exponentially in the x direction. We therefore assume that $NL \ll r$ as $r \to \infty$. Then we obtain in the leading order

$$A_- = 2\left(\frac{\pi v}{r}\right)^{1/2}\sum_{n=1}^{N(r)} e^{-vn^2L^2/4r}.$$

In the limit $r \to \infty$ the sum can be approximated by the integral

$$A_- = 2\left(\frac{\pi v}{r}\right)^{1/2} \int_0^\infty e^{-vn^2L^2/4r} dn = \frac{2\pi}{L}.$$

The total phase gradient at the point $(0, -\frac{r}{2})$ is therefore

$$\theta_x = A + \frac{2}{L}\left(\eta \sum_{n=0}^{\infty} K_0(n\eta) - \pi\right), \tag{10}$$

where $\eta = \frac{vL}{2}$. This value agrees well with the numerically computed gradient (to within six significant figures for $y \simeq 10^5$). Numerically, the negative (decelerating) term in (10) prevails over the first (accelerating) term in large parentheses when L is not very small. This is a consequence of a slow decay of the phase gradient behind the moving defect. As a result, the defects decelerate with decreasing L, as shown in Fig. 9. The effect of the far row of images would not be, of course, significant for defects moving towards annihilation, due to the rapid decay of the phase field ahead of the moving defect.

The above results demonstrate the feasibility of the semianalytical "particle-field" description of patterns with defects, incorporating the influence of sidewalls and external fields as well as of the defect interactions. The self-consistent velocities turned out to be quite close to the results of full nonstationary computations whenever comparisons could be drawn. Rather unexpected results obtained for the motion in the presence of lateral walls demonstrate strong effects of the asymmetry of the phase field of moving defects.

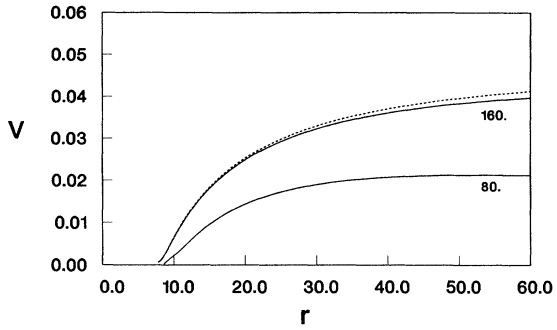

FIG. 9. Nucleation of a pair of defects under external phase gradient ($A = 0.1$) in the presence of lateral walls. The curves are labeled by the distance between the walls. The dashed line shows the $v(r)$ curve for the infinite domain.

This research was supported by the US–Israel Binational Science Foundation. J.D.R. acknowledges the support of the Lady Davis Foundation.

[1] E. Bodenschatz, W. Pesch, and L. Kramer, Physica D **32**, 135 (1988).
[2] G. Goren, I. Procaccia, S. Rasenat, and V. Steinberg, Phys. Rev. Lett. **63**, 1237 (1989).
[3] L.M. Pismen and J.D. Rodriguez, Phys. Rev. A **42**, 2471 (1990).
[4] E. Braun and V. Steinberg, Europhys. Lett. **15**, 167 (1991).